Parametric study of the particle motion induced by a vortex shaker

Marc Fischer, Somik Chakravarty, Olivier Le Bihan, Martin Morgeneyer

Parametric study of the particle motion induced by a vortex shaker

Marc Fischer[a,*], Somik Chakravarty[b], Olivier Le Bihan[d], Martin Morgeneyer[c]

[a] *Mines de Saint-Étienne, CNRS, UMR 5307 LGF, Centre SPIN, F-42023 Saint-Étienne, Université de Lyon, France*
[b] *Steinbeis R-Tech GmbH, Haus der Wirtschaft, Willi-Bleicher-Str. 19, 70174 Stuttgart, Germany*
[c] *Université de Technologie de Compiègne (UTC) Sorbonne Universités, Laboratoire Transformations intégrées de la matière renouvelable (TIMR), Rue Roger Couttolenc, CS 60319, 60203 Compiègne Cedex, France*
[d] *Institut National de l EnviRonnement Industriel et des RisqueS (INERIS), NOVA/CARA/DRC/INERIS, Parc Technologique Alata, BP2, F-60550 Verneuil-En-Halatte, France*

Keywords:
PEPT Powder Vortex-shaker Dustiness

Abstract Vortex shakers can be used to study the dustiness of powders. A parametric study has been performed to estimate the influence of diverse features on a traced particle's movements. The air flow has almost no effect on the particle's motion. Increasing the powder mass from 2 g to 4 g has no effect on the horizontal coordinates but increases the height and tends to decrease the velocity. Using a larger tracer particle does not affect the height but it increases the width of the horizontal coordinates and the velocity. Increasing the rotation speed from 1000 rpm to 2500 rpm has contradictory consequences. The effects on the other variables are unsystematic and depend on whether 2 g or 4 g of powder have been used. Plausible explanations could be offered for several of the trends but numerical modelling will be necessary for accounting for all findings.

1. Introduction

The use, the handling and the transportation of powders is often accompanied by the release of dust particles [1]. Dust aerosols are small solid particles, conventionally defined as those particles below 75 μm in diameter, which settle out under their own weight but which may remain suspended for some time, according to the International Standardisation Organisation (ISO 4225 - ISO, 1994) [2]. The tendency of a powder to generate dust is known as its dustiness, which is a function of both its physical properties and of the characteristics of the process and corresponds to the ratio between cohesion forces and separation forces [3]. Dust emissions from powders are deeply problematic from the standpoint of disease prevention [4], explosion risk management [5] and economic loss minimisation [6] . A good way to reduce them would be the development of predictive models dependent on the physical parameters used to describe the powder and the process in question [7, 8]. Meso-scale lab testers are utilised to simulate diverse

*Corresponding author: marc.fischer@emse.fr

industrial processes [1]. While the dustiness testers are usually conceived in such a way that the input energy and dust generation mechanisms are close to industrial situations [9, 10], there are only few works which straightforwardly compare the experimental and industrial conditions [11]. This limits our ability to understand, simulate and predict dustiness under industrially relevant circumstances [12].

One widespread dustiness technique is the free falling method where a powder is released on top of a test chamber and falls through the action of gravity [13]. Another technique is the rotating drum where a powder is placed in a drum whose rotation axis is horizontal [14]. Both techniques require a relatively large amount of powder (such as 50 g) [15, 16]. The Vortex Shaker Dustiness Tester (VS) represents an alternative to these two approaches [17]. As in the case of the rotating drum, the powder is strained through rotation but this time along the axis of a vertically placed test tube (see Figure 1). Besides allowing one to investigate situations that are not captured by the rotating drum, it can be employed with a significantly lower quantity of powder (2 g). It has been successfully used for investigating the aerosolisation of fine alumina powders [17], calcium carbonate powders [7] and of a carbon nanotube bulk [9] and further works are ongoing. The next step would consist of developing predictive numerical models that can deduce dust emissions from a given powder as a function of its features and the parameters of the VS [8]. This demands first a thorough understanding of the particles' trajectory within the rotating test tube, as dust is usually generated during particle-particle and particle-wall collisions [7].

To obtain the relevant experimental measurements, we used PEPT (Positron Emission Particle Tracking) [18] to follow the behaviour of a traced alumina particle over a period of 700 s at the standard operating conditions (namely $\omega = 1{,}500$ rpm with an air flow going through the test tube and 2 g of powder). The results we already obtained [8] (and that are to be shortly described in Section 2) gave us deep insights into the nature of the particle's motion within the test tube. In the current study, we endeavoured to better our understanding of the tester through a parametric study whereby the influence of the powder mass, of the rotation speed, of the traced particle's size, and of the closing of the test tube were investigated, respectively. The influence of these parameters on the movements of the traced particle was systematically studied and interpretations of the different trends have been offered.

In Section 2, we go into the methodology of the present study and our former results. In Section 3, we present the results of the parametric study along with their potential interpretations. Finally, in Section 4, conclusions are presented and an outlook for the future is given.

2. Experimental foundation and prior results

2.1. Test protocol

The utilisation of a vortex shaker as a technique for the generation of dust particles out of powders is a relatively novel and promising approach whose advantage is to be able to employ very small amounts of powder [9, 17]. This renders the VS method a practical and cheap dustiness tester in comparison to the standardised dustiness testers comprising the rotating drum [19] and the dropping test [20]. A vortex shaker can be viewed in Figure 1. The vortex shaker utilised for this investigation consists of a digital vortex shaker (VWR Signature Digital Vortex Mixer, USA). Such shakers or mixers are often used in laboratories to mix up small amounts of liquids. It is made of an electric motor with a drive shaft oriented vertically, which is connected to a rubber cup mounted slightly off-centre (orbital length 4.5 mm). Dust is generated from a small quantity (around 2 g) of bulk solid sample contained in a glass centrifuge tube (diameter 0.025 m, height 0.150 m) firmly mounted on the rubber cup. As the motor runs, the rubber cup oscillates rapidly in a circular movement and the motion is transmitted to the solid sample inside the cylindrical tube. The shaker is able to generate a uniform vortex action with rotational velocities ranging from 500 rpm to 2,500 rpm along the vertical axis. Due to the centrifugal forces spawned in the vortex shaker set-up, the particles in the bulk sample can be assumed to be subjected to the outward centrifugal force acting as a separation force, the vertical gravitational force and surface forces between the particles binding them together. The powder bed is initially located at the bottom of the test tube. The position of an alumina particle has been traced by using the technique PEPT [21–23] that provides one with a highly noisy temporal trajectory [8]. In our last article, we wanted to study the behaviour of limestone powders ($CaCO_3$). Since limestone primary particles could not be marked radioactively, we used instead a gamma-alumina particle (Al_2O_3) with similar physical properties to those of the powder. For the present parametric study, we decided to only use gamma-alumina for the sake of consistency, which means that both the powders and the tracer particles were made of alumina and have the very same physical properties. The alumina powder is sieved for 3 different sizes, namely 50 μm, 80 μm and 150 μm. A particle is selected between 50 and 80 μm (and referred to as small) whereas another particle (referred to as big) is selected between 80 and 150 μ.

One particle of the powder is radio-activated and followed by the detector camera thanks to its regular emissions of gamma rays. The experiments were performed at the Positron Imaging Centre, Nuclear Physics research group, University of Birmingham. The reader is referred to our previous publication for more details about the experimental setup [8]. The primary size distribution of the alumina powder remains always the same and is characterised by the

following values: $d_{10} = 57.55$ μm, $d_{25} = 63.64$ μm, $d_{50} = 70.43$ μm, $d_{75} = 76.13$ μm, and $d_{90} = 80.75$ μm. The size distribution of the sample used to produce the tracer p article, varies, however, between the "small" and the "big" tracer particle, as defined above. The particle density of the used alumina powder is 2950 kg.m^{-3}. The trial was always repeated once. The powder bed covered a height of 6 mm lying on the round bottom of the test tube.

2.2. Statistical methodology

The particle's movement is studied for the whole duration of the steady state that is only slightly shorter than the entire experiment (720 s). The population densities of the particle have been computed using all data as the frequency with which the particle is present in a given region. Since the motion of the particle has a cyclical shape whose "period" (roughly 1 s) is much inferior to the duration of the experiments, we can identify these frequencies with the population densities under the assumption of ergodicity [24]. To remove the experimental noise, we considered a displacement d as legitimate only if $d > d_{crit}$ where d_{crit} is a critical distance. As illustrated by Figure 2 (taken from our previous article [8], setting $d_{crit} = 5$ mm is a good compromise between erasing spurious pseudo-movements and keeping genuine tendencies. After the filtering, the velocity and velocity vectors (V, V_x, V_y, and V_z) are defined locally between two points of the filtered trajectory. The angle between two consecutive filtered vectors can be computed according to the formula

$$\phi = arccos(-\frac{\vec{a} \cdot \vec{b}}{|\vec{a}|\,|\vec{b}|}). \tag{1}$$

3. Results and discussion

In what follows, the effects of the powder mass, the size of the tracer particle, the deactivation of the air stream throughout the test tube and the rotation speed on the particle's behaviour have been investigated. The frequency distribution of the coordinates (x, y, z) and of the velocity vectors (V, V_x, V_y, and V_z) have been systematically computed along with the frequency with which two consecutive vectors form an angle smaller than 90°. The particle's kinetic energy E has only been considered for studying the influence of the particle size, as V contains all its information otherwise. All variables have been characterised by their third quartiles $Q_3(75\%)$ except V_y that is characterised by both its third quartile (V_y^+ for the upward movements) and its first quartile (V_y^- for the downward movements) because its frequency distribution is asymmetrical.

3.1. Powder mass

The effects of increasing the powder mass (and consequently the height of the powder bed) have been investigated at different rotation speeds while the test tube was open (i.e. while air was flowing through the top of the test tube at a speed included between 0.6 L.min^{-1} and 0.7 L.min^{-1}) and the tracer particle was small, as defined in Subsection 2.1. The effects on the horizontal coordinates and velocities are shown in Figure 3. The changes in the x and z directions are not significant. However, V_x and V_z are very much higher at 1000 rpm and 1500 rpm and insignificantly higher at 2000 rpm. At 1000 rpm and 1500 rpm, the values are more than three times higher for 2 g than for 4 g. The effects on the vertical coordinate and velocity are shown in Figure 4. The heights reached by the particle lying on 4 g of powder are 2 mm or more higher than those corresponding to 2 g of powder. The upward velocity (represented by the third quartile $Q_3(y)$) is considerably smaller for 4 g of powder. However, the downward velocity (represented by the first quartile $Q_1(y)$) is only significantly smaller for 4 g of powder at 1000 rpm.

Finally, Figure 5 shows the particle's speed V along with the proportion of abrupt changes in direction (defined as the angles inferior or equal to 90°), as defined above. Increasing the mass strongly decreases V at 1000 rpm and 1500 rpm but it has an insignificant effect at 2000 rpm. A powder mass of 4 g is associated with a higher proportion of sharp angles, whereby the increase is strong at 1500 and 1000 rpm but rather insignificant at 2000 rpm. The results of increasing the powder mass are summarised in Table 1.

The higher percentage of sharp angles might originate from a greater number of particle-particle collisions when 4 g of powder is present due to the higher particle concentration in the gas phase. This interpretation is supported by the work of Morgeneyer et al. [17] who investigated the aerosolisation of a pseudo-bimodal alumina powder and found that the aerosol mass concentration rises *more than linearly* in proportion to the sample mass. Such an effect could then be weaker at 2000 rpm where there is already a large number of collisions. The higher number of collisions would, in turn, considerably decrease the horizontal velocity $|V_x|$ and $|V_z|$ while having a more limited effect on the vertical velocity $|V_y|$, especially in the downward direction where gravity may play a role. Despite the lower $|V_y^+|$, the higher heights reached for 4 g can be well explained as the effect of significantly increasing the bed height.

3.2. Air stream through the test tube

The effects of closing the air stream flowing through the test tube (across an inlet and an outlet at its top at $y =$ 150 mm) have been investigated using a small tracer particle lying on 2 g of powder. Due to power limitation, we could not reach our usual value of 4.2 L.min^{-1} (utilised because of our specific cyclone) and had to content ourselves with

0.7 L.min^{-1}. The results are shown in Figures 6-8. It can be seen that the effects of switching off the air stream are negligible, except at 2000 rpm where it leads to less sharp angles although the variation range between two repeated trials for the open case is half as large as the difference between the closed and open case. Given the fact that all other variables are unaffected and that the opening is much higher than the highest heights reached by the particle (namely 20 mm), there does not appear to be any intuitive explanation for this anomaly other than its being an artefact stemming from the limitation of repeatability. Future simulations could shed light onto this result. Given that the inner diameter of the inlet tube is 3 mm and that the flow rate is 0.7 L.min^{-1}, the value of the velocity of the flow is 1.65 m.s^{-1}, which is industrially relevant [25]. This value approaches the velocity of the rotating test tube at 1500 rpm (1.884 m/s). Nevertheless, given the fact that the inlet and outlet are more than 100 mm above the powders surface [17], we can expect the flow to only have a small influence on the behaviour of the particle that only reaches heights inferior to 25 mm. Because of the limitations of the PEPT experimental setup, we could not use the usual value of 4.2 L.min^{-1} which is 6 times higher than 0.7 L.min^{-1}. As a consequence, we do not know if this higher flow rate could have a stronger influence on the particle's behaviour. The future CFD studies we plan to conduct will shed further light on the role of the flow rate value.

3.3. Size of the tracer particle

The role of the size of the tracer particle has been examined at 1500 rpm while the air stream was closed and 2 g of powder were used. The effects on the horizontal coordinate and velocity are shown in Figure 9. The big particle occupies a larger horizontal space and reaches stronger horizontal velocities. Figure 10 displays the effects on the vertical motion. Whilst the vertical volume the particle's movement takes up is not influenced by the particle's size, the bigger particle has a much lower upward and downward velocity. Figure 11 shows the particle's velocity V along with its kinetic energy and the proportion of abrupt changes in direction (defined as the angles inferior or equal to 90°). Increasing the size leads to a relatively higher velocity V and to a much stronger kinetic energy E and a larger number of sharp angles. The consequences of increasing the tracer particle's size are summarised in Table 2. We can tentatively formulate hypotheses to account for some of these observations. The higher values of the horizontal velocity when the tracer particle is large leads to a larger horizontal space occupied by the particle and thus to higher values of $|x|$ and $|z|$. The larger size of the tracer particle could make it more susceptible to undergo collisions, hence the higher proportion of sharp angles. These collisions could, in turn, lower the values of the vertical component of the velocity, both downwards and upwards. Since the decrease in $|V_y^-|$ and $|V_y^+|$ is roughly the same (namely approximately 10

mm/s), the heights reached by the particle remain unaffected.

The cause of the increase in $|V_x|$ and $|V_z|$ is harder to explain. The centrifugal force [26] is given by the following formula $F_c = m\,\omega^2\,R$, where m is the particle's mass, ω the (local) rotational speed of the particle and R the radius of its cyclic trajectory. Consequently, the acceleration it spawns is independent of the particle's mass and diameter and cannot be influenced by them. The drag force caused by the air on the particle [27] is given by the following formula $F_D = \frac{1}{2}\,\rho\,v^2\,C_D\,A$, where ρ is the density of the fluid v is the speed of the object relative to the fluid, A is the cross sectional area, and C_D is the drag coefficient. However, since the motion of the particle is generally not circular but is unknown at a given time t (see Fig. 2), we cannot know whether or not its trajectory is perpendicular to the radial axis of the Vortex Shaker. Figure 12 shows the horizontal velocity profile $V_x(x)$ for the small and the big particle. It can be seen that V_x is always considerably higher for the big particle than for the small one. One hypothesis might be that the big particle loses less velocity through collisions thanks to it larger mass. A more compelling explanation can be only discovered through numerical modelling.

3.4. Rotation speed

The effects of the rotation speed on the small and large particles have been investigated and are shown in Table 3. Some tendences can potentially be accounted for. In general, the decrease in the particle velocity under some conditions might be explained by an increase of interparticle forces that can considerably reduce the particle mobility owing to the larger amounts of particles produced by desaggregation due to the test tube rotation and vibration [28]. It also possible that the interference of the imparted vibrations of the Vortex Shaker with the natural frequencies of the powder system might also have a considerable effect on the particle's behaviour and speed [29, 30]. Nevertheless, we were not able to explain every detail of our observations in Subsection 3.4.

Figure 13 shows the horizontal coordinates and velocities. Under consideration of the uncertainty, $|x|$ and $|z|$ tend to decrease with higher rotation speeds. However, $|V_x|$ and $|V_y|$ follow two different trends for 2 g and 4 g. While they increase in the case of 4 g of powder, in the case of 2 g, they increase till 1500 rpm before decreasing. The height and vertical velocity are shown in Figure 14. The heights reached by the particle and both the upward and the downward velocities constantly rise with the rotation speed. Figure 15 shows the velocity V along with the sharp angles. With 4 g of powder, V remains constant between 1000 and 1500 rpm before increasing whereas with 2 g, V increases until 1500 rpm, decreases between 1500 rpm and 2000 rpm before increasing again at 2000 rpm. For 2 g of powder, the percentage of sharp angles increases constantly between 1000 and 2000 rpm before increasing abruptly between 2000

rpm and 2500 rpm. With 4 g of powder, the percentage of sharp angles increases until 1500 rpm before decreasing. The trends have been summed up in Table 3.

4. Conclusion and outlook

The vortex shaker is a promising dustiness tester which allows one to estimate the propensity of a powder to emit dust whilst only necessitating a small quantity of material (2 g) [17]. Understanding the physical factors responsible for dustiness and developing models permitting numerical predictions is extremely important as this could greatly diminish the cost of studies aiming at minimising the risks related to dust emission [31]. Since dust emissions are due to a complex set of particle-wall and particle-particle collisions and particle-fluid interactions, it is necessary to comprehend and to be able to predict the movements of the powder primary particles in the test tube agitated by the vortex shaker. This prompted us to undertake a series of PEPT experiments to measure the motion of a traced primary particle and grasp the influence of the parameters of the tester and of the powder on it. Our previous study [8] evidenced that, on average, the particle rises at the middle of the test tube at a small speed while descending near the walls much more rapidly. In the present work, we investigated the effects of closing the air stream through the test tube, of increasing the powder mass, the rotation speed and the size of the primary particle. Overall, the air stream considered for the experiments has a very small if not negligible effect on the particle's behaviour and hence also on dust generation. Increasing the powder mass (and thereby the powder bed height) tends to increase the heights reached by the particle and to decrease its velocity. Increasing the size of the tracer particle raises the velocity and the breadth of the horizontal coordinates. An increase in the rotation speed leads to a narrower range of horizontal coordinates but also to higher heights reached by the particle. Many of this observations can be well accounted for on intuitive grounds. Nevertheless, others (such as the oscillations of the particle's velocity with the rotation speed) do not lend themselves well to intuitive explanations. We intend to perform a CFD (Computational Fluid Dynamics) and DEM (Discrete Element Method) study modelling the system as both discrete particles within the gaseous phase (following the Eulerian-Lagrangian approach [32]) and as the powder being treated as a continuous phase (Eulerian-Eulerian approach [33]) and we expect these results to shed light on our counter-intuitive findings.

5. Acknowledgements

We acknowledge Dr. Thomas Leadbeater (who worked previously at the University of Birmingham in the UK), Dr. Pablo García-Tríñanes and Prof. David Parker for preparing and allowing the experiments at the University

of Birmingham. We would also like to acknowledge Prof. J.P.K. Seville (University of Surrey, UK) for his useful insights regarding the use of PEPT for this study. This work was supported by the European Union FP7 Marie Curie Actions Initial Training Network T-MAPPP (Training in Multiscale Analysis of MultiPhase Particulate Processes and Systems) under grant agreement No 607453 and the Region Picardie/ Hauts de France and by the Programme 190 (French Ministry of Environment). We solemnly declare that there are no conflicts of interest.

References

[1] F. Hamelmann, E. Schmidt, Methods of estimating the dustiness of industrial powders–a review, KONA Powder and Particle Journal 21 (2003) 7–18.

[2] E. Petavratzi, S. Kingman, I. Lowndes, Particulates from mining operations: A review of sources, effects and regulations, Minerals Engineering 18 (2005) 1183–1199.

[3] M. Plinke, B. Homburg, Vorhersage der Staubentstehung bei der industriellen Handhabung von Pulvern, VDI, 1995.

[4] T. Kraus, K. Schaller, J. Angerer, S. Letzel, Aluminium dust-induced lung disease in the pyro-powder-producing industry: detection by high-resolution computed tomography, International archives of occupational and environmental health 73 (2000) 61–64.

[5] R. K. Eckhoff, Dust explosions in the process industries: identification, assessment and control of dust hazards, Gulf professional publishing, 2003.

[6] H. Y. Aruntaş, M. Gürü, M. Dayı, I. Tekin, Utilization of waste marble dust as an additive in cement production, Materials & Design 31 (2010) 4039–4042.

[7] S. Chakravarty, O. Le Bihan, M. Fischer, M. Morgeneyer, Dust generation in powders: Effect of particle size distribution, in: EPJ Web of Conferences, volume 140, EDP Sciences, p. 13018.

[8] S. Chakravarty, M. Fischer, P. García-Triñanes, D. Parker, O. Le Bihan, M. Morgeneyer, Study of the particle motion induced by a vortex shaker, Powder Technology (2017).

[9] O. L. C. Le Bihan, A. Ustache, D. Bernard, O. Aguerre-Chariol, M. Morgeneyer, Experimental study of the aerosolization from a carbon nanotube bulk by a vortex shaker, Journal of Nanomaterials 2014 (2014) 7.

[10] Y. Ding, B. Stahlmecke, H. Kaminski, Y. Jiang, T. A. Kuhlbusch, M. Riediker, Deagglomeration testing of airborne nanoparticle agglomerates: Stability analysis under varied aerodynamic shear and relative humidity conditions, Aerosol Science and Technology 50 (2016) 1253–1263.

[11] S. Kamath, V. Puri, H. Manbeck, R. Hogg, Flow properties of powders using four testersmeasurement, comparison and assessment, Powder technology 76 (1993) 277–289.

[12] W. A. Heitbrink, W. F. Todd, T. C. Cooper, D. M. O'Brien, The application of dustiness tests to the prediction of worker dust exposure, The American Industrial Hygiene Association Journal 51 (1990) 217–223.

[13] W. A. Heitbrink, P. A. Baron, K. Willeke, An investigation of dust generation by free falling powders, The American Industrial Hygiene Association Journal 53 (1992) 617–624.

[14] R. G. Sherritt, J. Chaouki, A. K. Mehrotra, L. A. Behie, Axial dispersion in the three-dimensional mixing of particles in a rotating drum reactor, Chemical Engineering Science 58 (2003) 401–415.

[15] N. Breum, The rotating drum dustiness tester: variability in dustiness in relation to sample mass, testing time, and surface adhesion, Annals of Occupational Hygiene 43 (1999) 557–566.

[16] M. Boundy, D. Leith, T. Polton, Method to evaluate the dustiness of pharmaceutical powders, Annals of Occupational Hygiene 50 (2006) 453–458.

[17] M. Morgeneyer, O. Le Bihan, A. Ustache, O. Aguerre-Chariol, Experimental study of the aerosolization of fine alumina particles from bulk by a vortex shaker, Powder Technology 246 (2013) 583–589.

[18] M. Tan, D. Parker, P. Dee, Pept data presentation software, manual, Birmingham University, UK (1997).

[19] D. Parker, A. Dijkstra, I. Martin, J. P. K. Seville, Positron emission particle tracking studies of spherical particle motion in rotating drums, Chemical Engineering Science 52 (1997) 2011–2022.

[20] S. Bach, E. Schmidt, Determining the dustiness of powdersa comparison of three measuring devices, Annals of occupational hygiene 52 (2008) 717–725.

[21] M. Van de Velden, J. Baeyens, J. P. K. Seville, X. Fan, The solids flow in the riser of a Circulating Fluidised Bed (CFB) viewed by Positron Emission Particle Tracking (PEPT), Powder Technology 183 (2008) 290–296.

[22] D. Valdesueiro, P. Garcia-Triñanes, G. Meesters, M. Kreutzer, J. Gargiuli, T. Leadbeater, D. Parker, J. Seville, J. van Ommen, Enhancing the activation of silicon carbide tracer particles for pept applications using gas-phase deposition of alumina at room temperature and atmospheric pressure, Nuclear Instruments and Methods in Physics Research Section A: Accelerators, Spectrometers, Detectors and Associated Equipment 807 (2016) 108–113.

[23] M. Marigo, M. Davies, T. Leadbeater, D. L. Cairns, A. Ingram, E. H. Stitt, Application of Positron Emission Particle Tracking (PEPT) to validate a Discrete Element Method (DEM) model of granular flow and mixing in the Turbula mixer, International journal of pharmaceutics 446 (2013) 46–58.

[24] T. Royama, Analytical population dynamics, volume 10, Springer Science & Business Media, 2012.

[25] G. Belforte, M. Carello, V. Viktorov, Fluidised bed for stripping sand casting process, in: 67th Word Foundry Congress Harrogate (UK), pp. 5–7.

[26] M. A. Abramowicz, Centrifugal force-a few surprises, Monthly Notices of the Royal astronomical society 245 (1990) 733.

[27] G. K. Batchelor, An introduction to fluid dynamics, Cambridge university press, 2000.

[28] H. Salehi, N. Lotrecchiano, D. Barletta, M. Poletto, Dust release from aggregative cohesive powders subjected to vibration, Industrial & Engineering Chemistry Research 56 (2017) 12326–12336.

[29] D. Barletta, M. Poletto, Aggregation phenomena in fluidization of cohesive powders assisted by mechanical vibrations, Powder technology 225 (2012) 93–100.

[30] D. Barletta, P. Russo, M. Poletto, Dynamic response of a vibrated fluidized bed of fine and cohesive powders, Powder technology 237 (2013) 276–285.

[31] L. E. Stone, P. W. Wypych, D. B. Hastie, S. Zigan, et al., Cfd-dem modelling of powder flows and dust generation mechanisms-a review, in: 12th International Conference on Bulk Materials Storage, Handling and Transportation (ICBMH 2016), The, Engineers Australia, p. 417.

[32] B. Van Wachem, J. Van der Schaaf, J. Schouten, R. Krishna, C. Van den Bleek, Experimental validation of lagrangian–eulerian simulations of fluidized beds, Powder Technology 116 (2001) 155–165.

[33] D. Santos, I. Petri, C. Duarte, M. Barrozo, Experimental and cfd study of the hydrodynamic behavior in a rotating drum, Powder technology 250 (2013) 52–62.

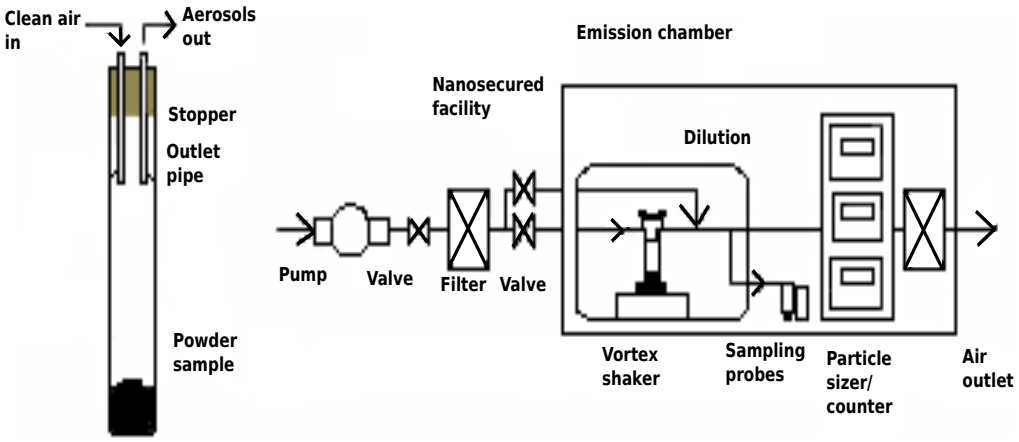

Figure 1: The vortex shaker experiment [17]

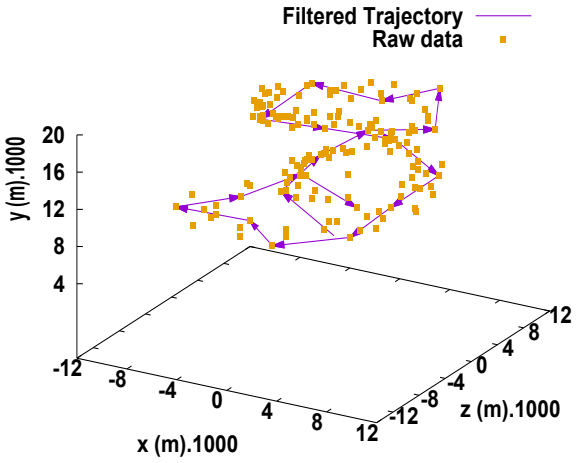

Figure 2: Filtered trajectory

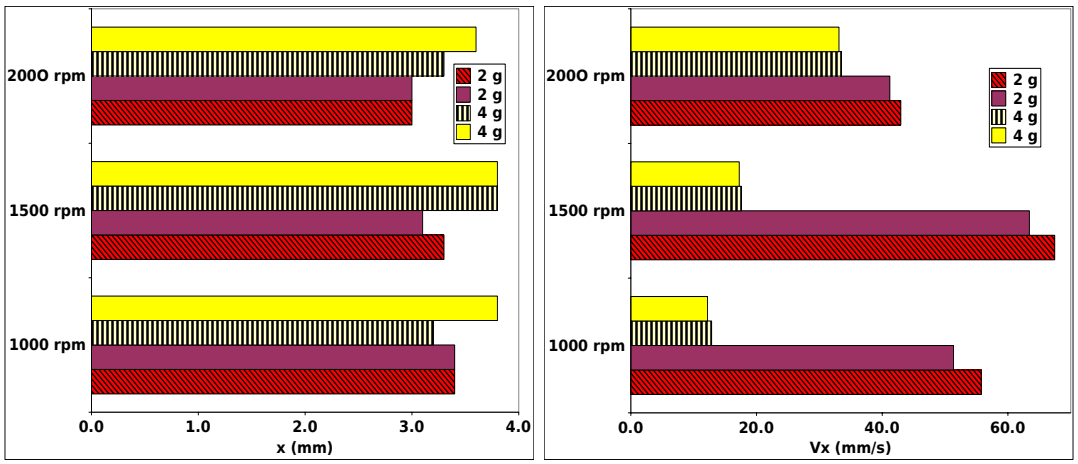

(a) $Q_3(x)$ (b) $Q_3(V_x)$

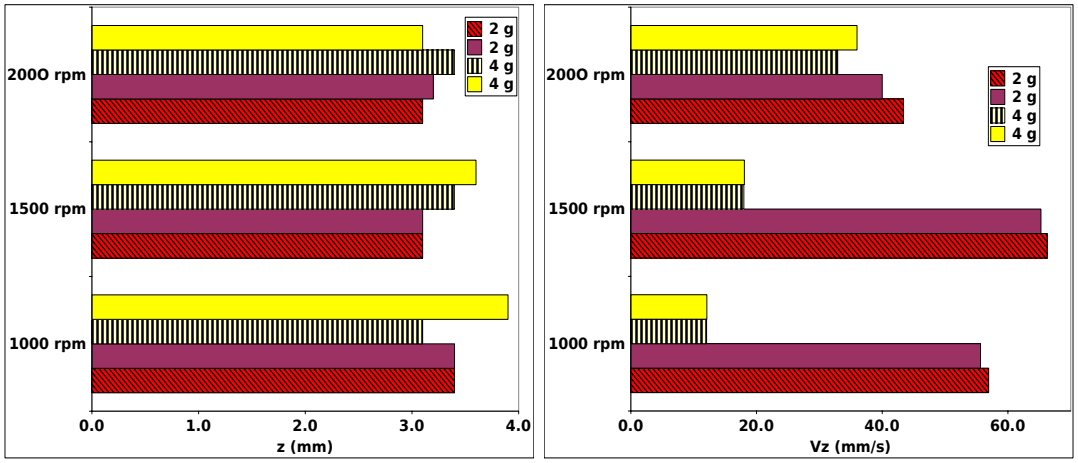

(c) $Q_3(z)$ (d) $Q_3(V_z)$

Figure 3: Effects of the powder mass on the horizontal coordinates and velocities

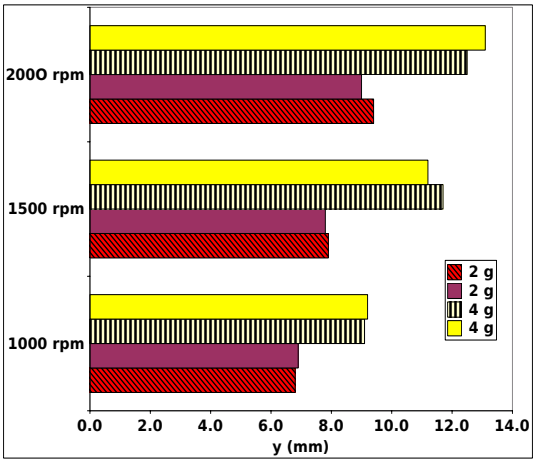

(a) $Q_3(y)$

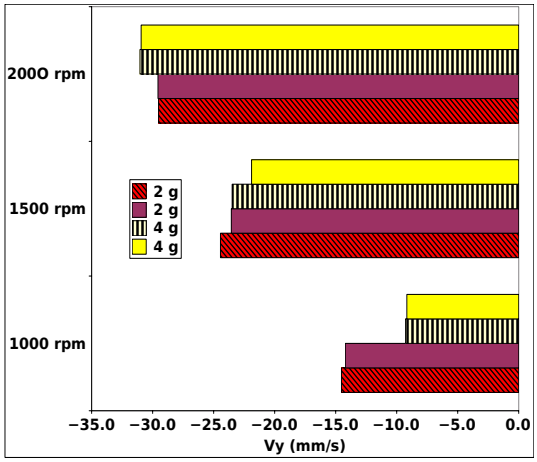

(b) $Q_1(V_y)$

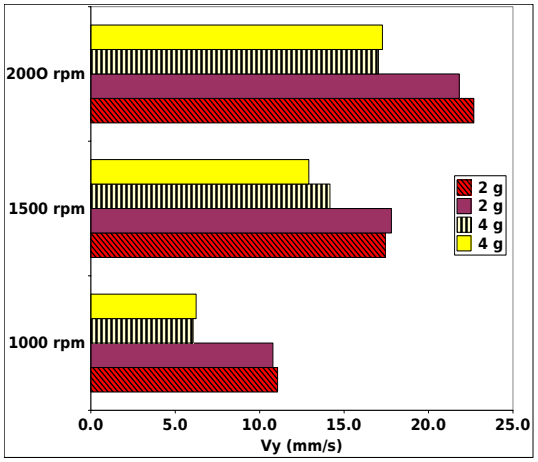

(c) $Q_3(V_y)$

Figure 4: Effects of the powder mass on the height and vertical velocity

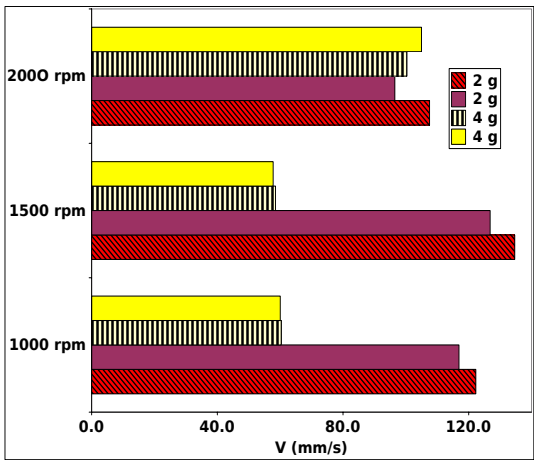

(a) $Q_3(V)$

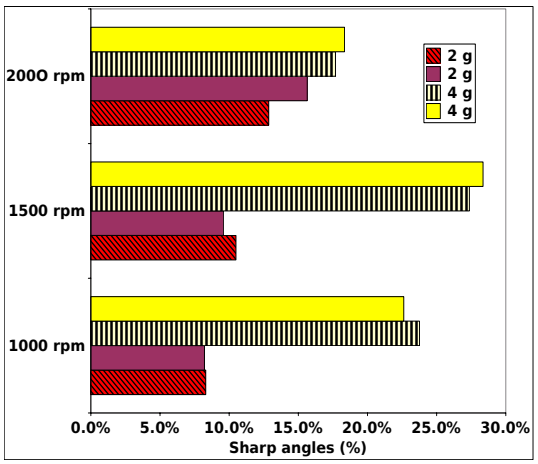

(b) Angles sharper than 90°

Figure 5: Effects of the powder mass on the velocity and sharp angles

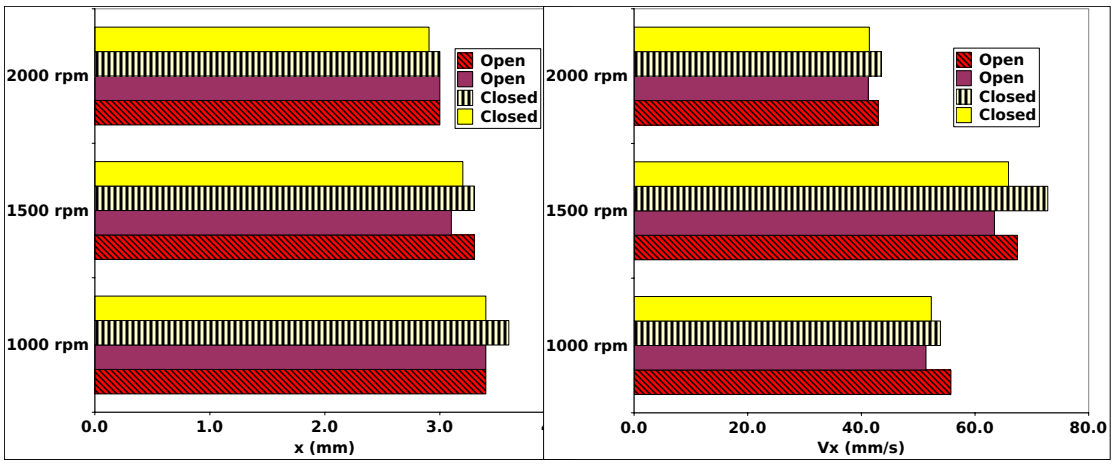

(a) $Q_3(x)$ (b) $Q_3(V_x)$

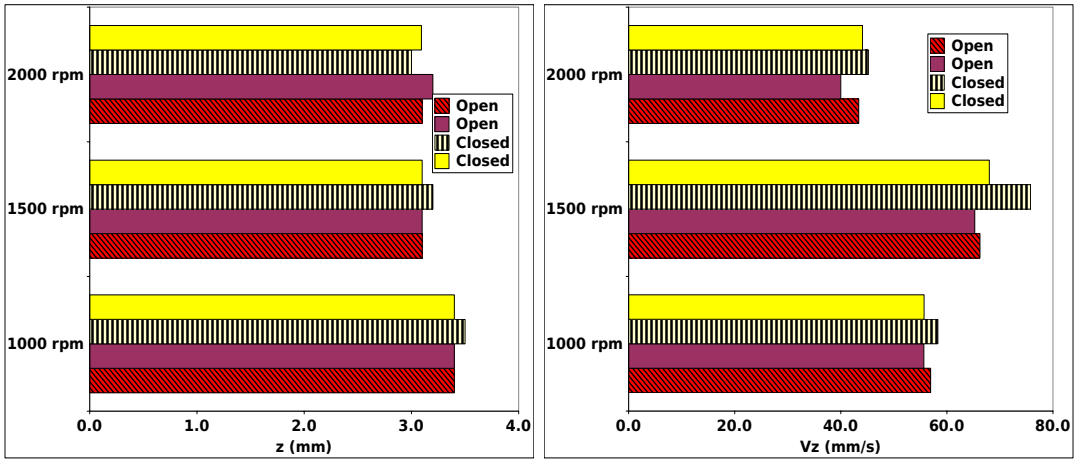

(c) $Q_3(z)$ (d) $Q_3(V_z)$

Figure 6: Effects of the air stream on the horizontal coordinates and velocities

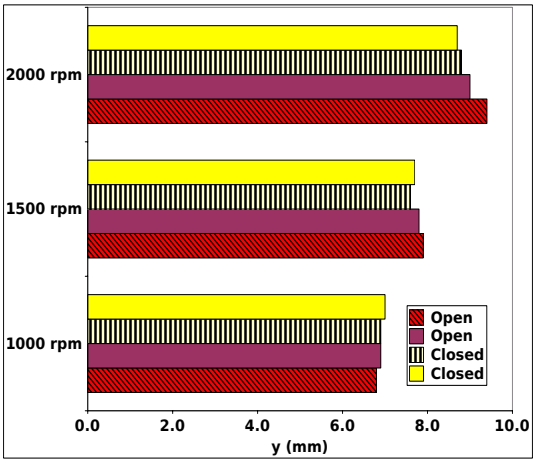

(a) $Q_3(y)$

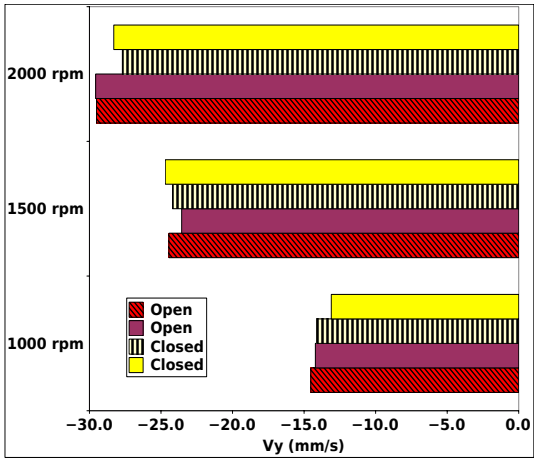

(b) $Q_1(V_y)$

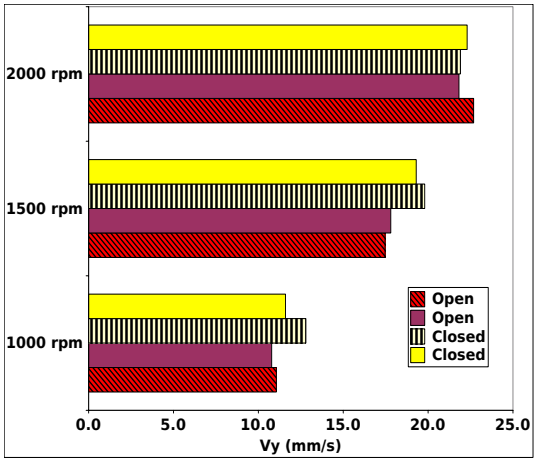

(c) $Q_3(V_y)$

Figure 7: Effects of the air stream on the height and vertical velocity

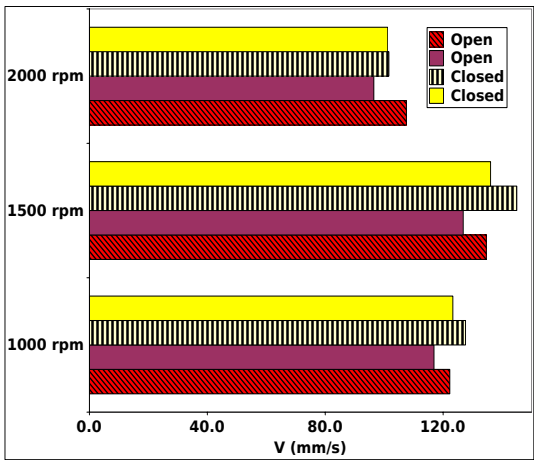

(a) $Q_3(V)$

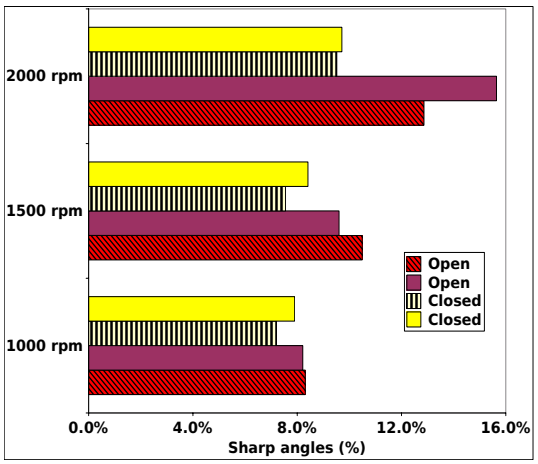

(b) Angles sharper than 90°

Figure 8: Effects of the air stream on the velocity and sharp angles

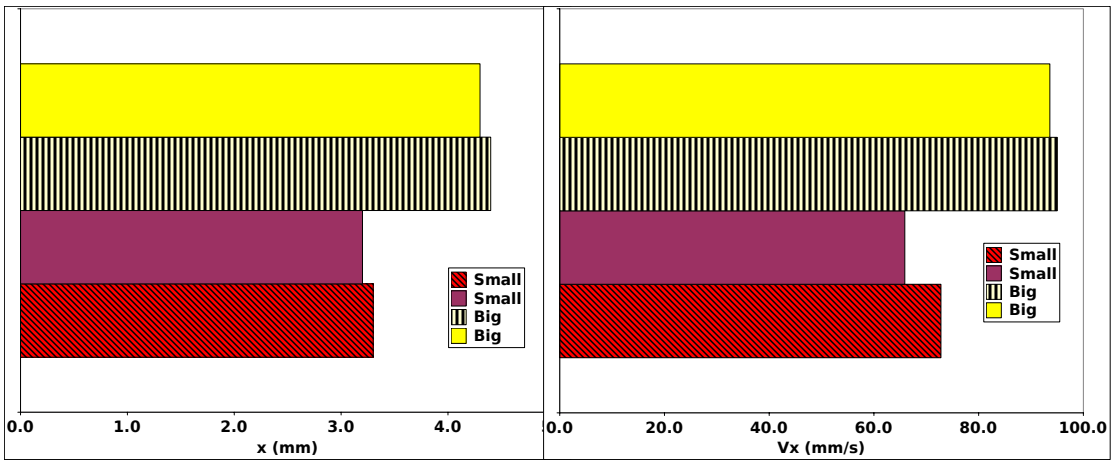

(a) $Q_3(x)$ (b) $Q_3(V_x)$

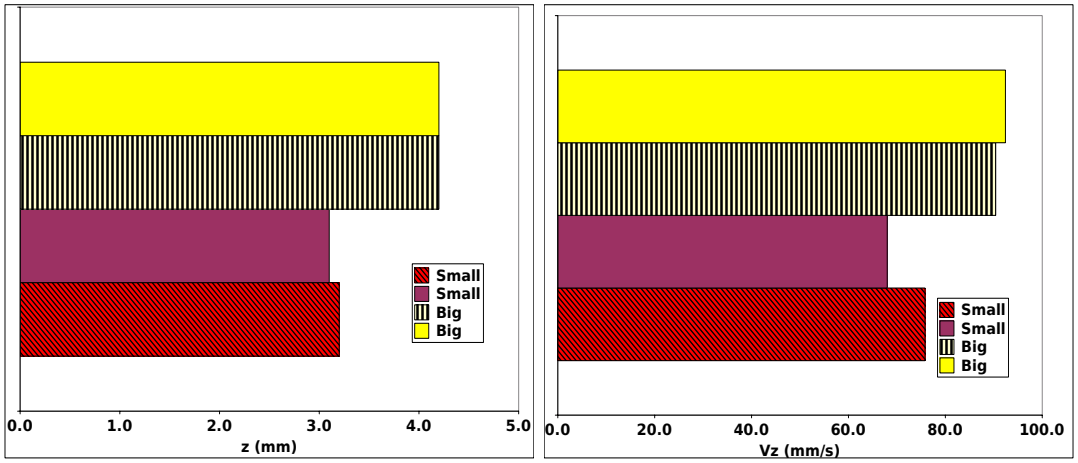

(c) $Q_3(z)$ (d) $Q_3(V_z)$

Figure 9: Effects of the particle size on the horizontal coordinates and velocities

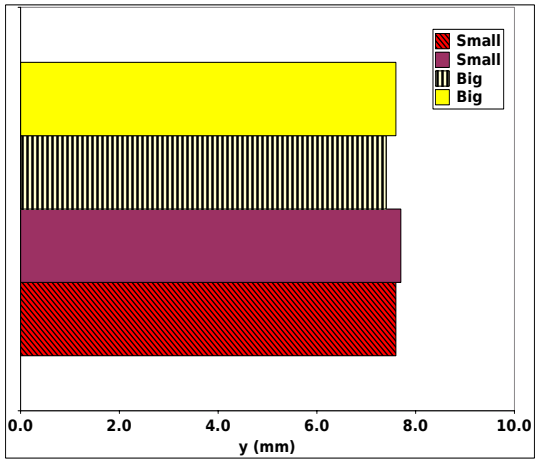

(a) $Q_3(y)$

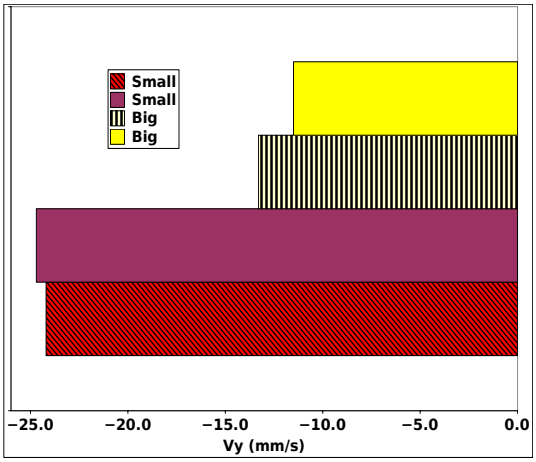

(b) $Q_1(V_y)$

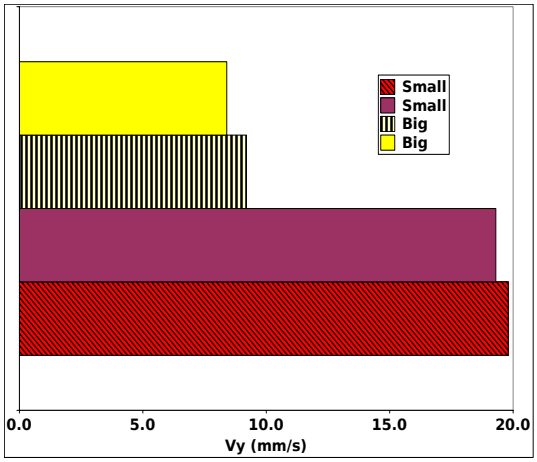

(c) $Q_3(V_y)$

Figure 10: Effects of the particle size on the height and vertical velocity

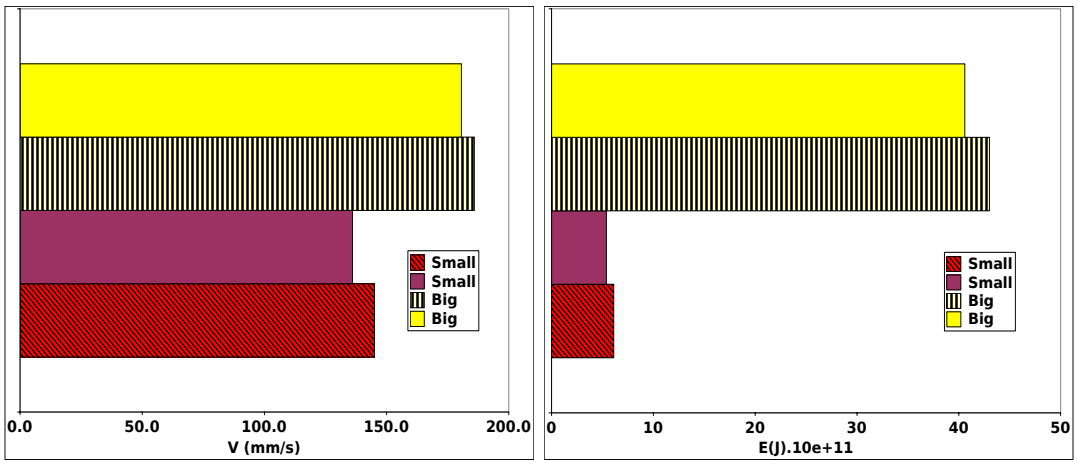

(a) $Q_3(V)$ (b) Kinetic energy

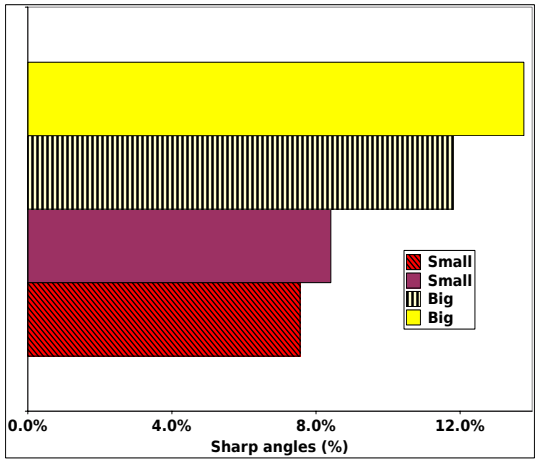

(c) Angles sharper than 90°

Figure 11: Effects of the particle size on the velocity and sharp angles

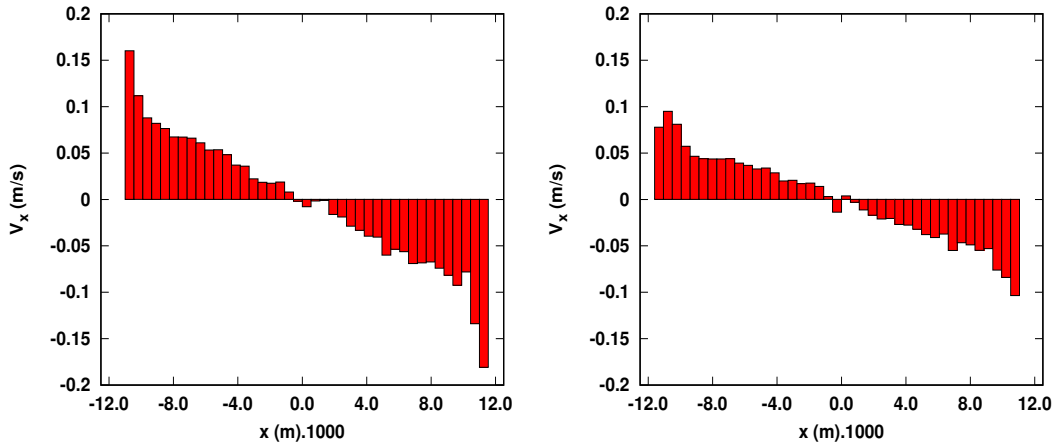

(a) Big particle (b) Small particle

Figure 12: V_x as function of x

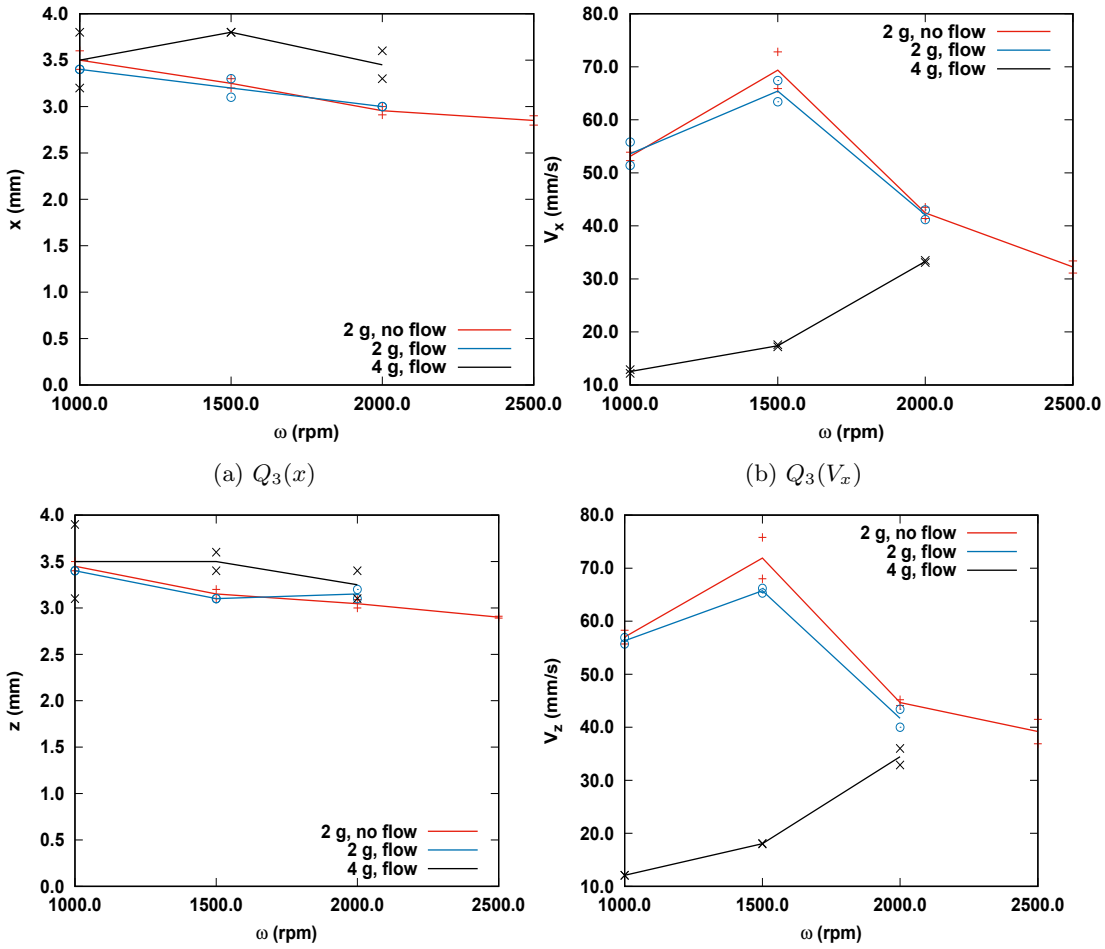

(a) $Q_3(x)$ (b) $Q_3(V_x)$

(c) $Q_3(z)$ (d) $Q_3(V_z)$

Figure 13: Effects of the rotation speed on the horizontal coordinates and velocities

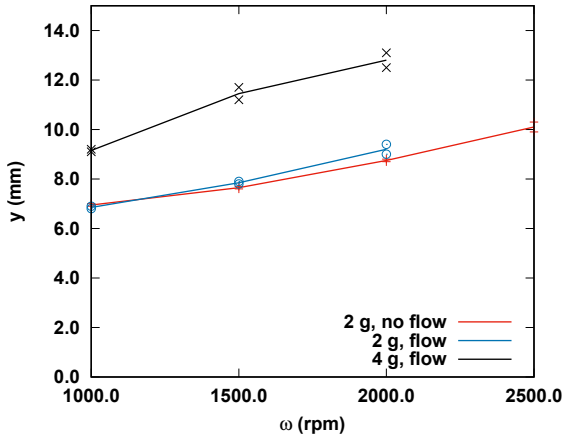

(a) $Q_3(y)$

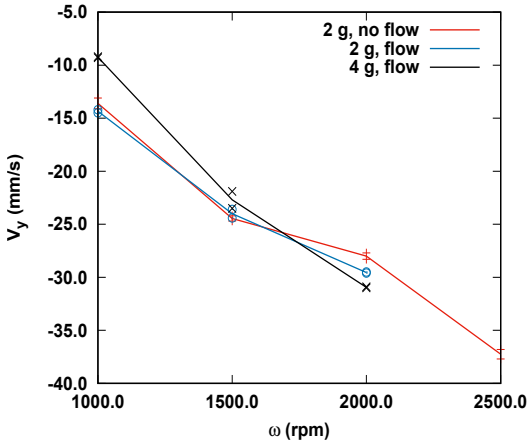

(b) $Q_1(V_y)$

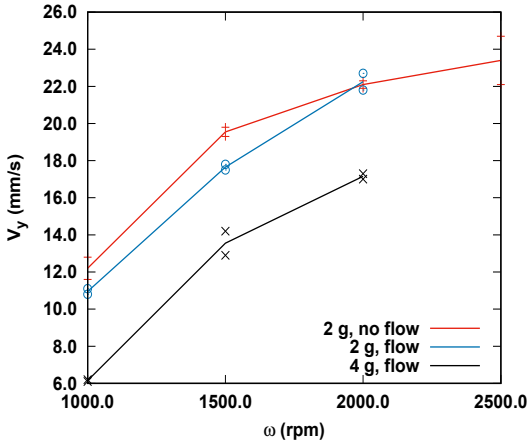

(c) $Q_3(V_y)$

Figure 14: Effects of the rotation speed on the vertical coordinates and velocities

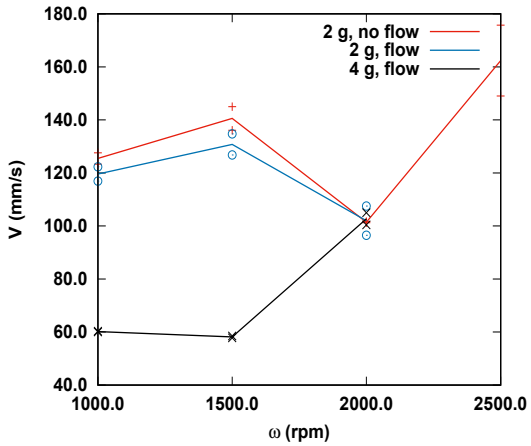

(a) $Q_3(V)$

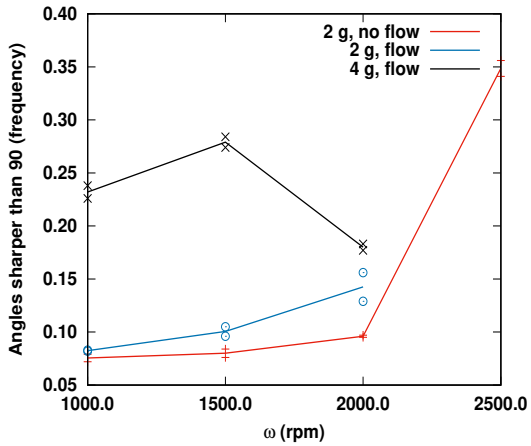

(b) Angles sharper than 90°

Figure 15: Effects of the rotation speed on the velocity V and sharp angles

Table 1: Effects of increasing the powder mass from 2 g to 4 g

Variable	1000 rpm	1500 rpm	2000 rpm
$\|x\|$, $\|z\|$	Insignificant	Insignificant	Insignificant
$\|y\|$	Higher	Higher	Higher
$\|V_x\|$, $\|V_z\|$	Much lower	Much lower	Slightly lower
$\|V_y^+\|$	Lower	Lower	Lower
$\|V_y^-\|$	Lower	Insignificant	Insignificant
V	Much lower	Much lower	Insignificant
Sharp angles	Much more	Much more	Slightly more

Table 2: Effects of increasing the tracer particle's size from small (50-80 μm) to large (80-150 μm)

Variable	Effect
$\|x\|$, $\|z\|$	Increase
$\|y\|$	Unchanged
$\|V_x\|$, $\|V_z\|$	Increase
$\|V_y^+\|$	Lower
$\|V_y^-\|$	Lower
V	Increase
E	Strong increase
Sharp angles	Much more

Table 3: Effects of increasing the rotation speed

Variable	2 g	4 g
$\|x\|$,$\|z\|$	Smaller	Smaller
$\|y\|$	Larger	Larger
$\|Vx\|$,$\|Vz\|$	Peak at 1500 rpm	Larger
$\|V_y^+\|$	Larger	Larger
$\|V_y^-\|$	Larger	Larger
V	Increases, decreases, increases	Increases, abruptly increases
Sharp angles	Increases, abruptly increases	Peak at 1500 rpm